Heliyon 10 (2024) e38586

Contents lists available at ScienceDirect

Heliyon

journal homepage: www.cell.com/heliyon

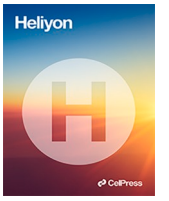

Review article

Noise characteristics of semiconductor lasers with narrow linewidth

Hua Wang [a,b], Yuxin Lei [a,*], Qiang Cui [a,b], Siqi Li [a,b], Xin Song [a,b], Yongyi Chen [a,c], Lei Liang [a], Peng Jia [a], Cheng Qiu [a], Yue Song [a], Yubing Wang [a], Yiran Hu [a,b], Li Qin [a], Lijun Wang [a]

[a] *State Key Laboratory of Luminescence Science and Technology, Changchun Institute of Optics, Fine Mechanics and Physics, Chinese Academy of Sciences, Changchun, 130033, China*
[b] *Daheng College, University of Chinese Academy of Sciences, Beijing, 100049, China*
[c] *Jiguang Semiconductor Technology Co., Ltd., Changchun, 130033, China*

ARTICLE INFO

Keywords:
Semiconductor lasers
Relative intensity noise
Phase noise
Narrow linewidth
Low noise

ABSTRACT

Narrow-linewidth semiconductor lasers are highly valued in scientific research and industrial applications owing to their high coherence and low phase noise characteristics, particularly in high-performance optical communications, sensing, and microwave photonic systems. Accuracy, a key objective of many application systems, is determined by the noise of the light source. As system accuracy improves, the requirements for the light source become more stringent, with linewidth reduction and noise reduction being the top priorities. Currently, extensive attention and research are focused on suppressing noise generated by narrow-linewidth lasers. This paper presents noise measurement methods, analyses of the mechanisms for noise suppression, and recent research progress in low-noise semiconductor lasers, focusing on material optimization, structural design, and feedback control. The limitations of current technological solutions are discussed, and future scientific trends are outlined.

1. Introduction

Narrow-linewidth low-noise semiconductor lasers are high-performance light sources with advantages of high spectral purity, high-frequency stability, and precise wavelength. They play indispensable roles in cutting-edge applications, such as optical communication systems [1–5], microwave photon systems [6–10], and sensing systems [11–15]. Accuracy is crucial in application systems, and the noise of light sources significantly determines the accuracy of the optical system. With the rapid advancement of artificial intelligence technology, there has been a significant increase in the demand for large-scale data processing and implementation analysis. Optical chips must be able to support higher data transmission rates and larger bandwidth capacity. The noise characteristics will have a crucial impact and even become a decisive factor.

Generally, the noise of semiconductor lasers includes phase noise, intensity noise, and frequency noise. Phase noise describes the random fluctuation of the laser output optical signal phase with time. Phase noise mainly comes from spontaneous radiation and carrier fluctuation, which are embodied as white noise and 1/f noise, respectively, and adversely affect the sensitivity of interferometry

* Corresponding author.
E-mail address: leiyuxin@ciomp.ac.cn (Y. Lei).

https://doi.org/10.1016/j.heliyon.2024.e38586
Received 23 September 2024; Received in revised form 26 September 2024; Accepted 26 September 2024
Available online 3 October 2024

and coherent optical communication systems. Intensity noise describes the random fluctuation of the intensity of the laser output optical signal. Intensity noise is mainly caused by spontaneous radiation, carrier fluctuation, temperature fluctuation, and is usually characterized by relative intensity noise (RIN), which has important impacts on the modulation characteristics, optical power stability, and optical signal transmission quality. Frequency noise describes the random change of the laser output optical signal frequency with time and is usually caused by changes in temperature, current, pressure, etc. The existence of frequency noise will lead to frequency drift of optical signals, affecting the stability and reliability of lasers.

Previously, linewidth characteristics of lasers has been significantly emphasized. With the development of technology, system performance improvement, and application scenario changes, light source noise has emerged as a significant challenge. In optical communication, noise affects the signal quality, transmission distance, system bandwidth, and transmission rate of the system [16]. In microwave photonics, it affects the signal-to-noise ratio, dynamic range, and system stability [17]. Moreover, noise determines the detection accuracy, detection distance, anti-interference ability, and stability of LiDAR systems [18].

Owing to the increasing application demands, noise measurement and suppression for semiconductor lasers has become a research hotspot. Technical solutions of noise suppression based on material optimization, structure design, and feedback control are constantly being proposed. This paper presents a thorough analysis of the noise generation mechanism and comprehensively summarizes the existing technical solutions to provide a scientific outlook on the development of semiconductor laser noise suppression technology.

2. Noise in semiconductor lasers

Noise in semiconductor lasers can be described as intensity or phase (frequency) noise. In an ideal scenario, the assumptions are that no spontaneous radiation occurs in the semiconductor laser and that the laser light is generated entirely by the stimulated radiation. This situation results in a stable output frequency and phase for a single-mode laser, and the output light can be expressed as:

$$E = E_{0e}^{j(\omega 0 t+\varphi 0)}, \tag{1}$$

where E_0 denotes the initial amplitude, ω_0 denotes the initial angular frequency, and φ_0 denotes the initial phase. However, spontaneous radiation is inevitable in actual output lasers. A laser generated by spontaneous radiation has a specific intensity and phase. The photons generated by spontaneous radiation randomly introduce a part of the field component into the coherent field generated by stimulated radiation because of irregularity and randomness, which can alter the amplitude and phase [19].

Generally, the normalized RIN is used to characterize the intensity noise as follows:

$$RIN = \frac{1}{B}\frac{\triangle P(\omega)^2}{P^2}, \tag{2}$$

where $\Delta P(\omega)^2$ is the mean-square optical intensity fluctuation at a defined frequency, P is the average output optical intensity, and B is the equivalent bandwidth. The unit of RIN is dBc/Hz, and this quantity characterizes the fluctuation of signal power [20]. The phase noise of semiconductor lasers is typically defined using the noise power spectral density (PSD), as follows:

$$S_\phi(f) = \phi^2(f)\frac{1}{BW}, \tag{3}$$

where BW is the bandwidth of the measurement system, and ϕ (f) is the phase noise deviation. The unit of $S_\phi(f)$ can be expressed as rad^2/Hz or Hz^2/Hz, and it characterizes the amount of variation in the Fourier frequency noise at different frequencies.

The relation between phase noise and frequency noise is as follows:

$$\varphi(t) = \int_0^t 2\pi\omega(\tau)d\tau. \tag{4}$$

Given that frequency is a differential of phase, the relationship between phase noise PSD and frequency noise PSD is as follows:

$$S_v(f) = f^2 S_\varphi(f). \tag{5}$$

According to Eq. (4), the frequency and phase noises can be transformed into each other and are essentially the same. Therefore, the noise in a single-mode laser is mainly described as intensity and phase (frequency) noise. The essential causes are the changes in the photon and carrier densities. The fluctuation in photon density leads to variation in the output power amplitude, whereas a change in the carrier density leads to variation in the refractive index, which further causes a change in the output wavelength, thus leading to phase (frequency) variation.

Spontaneous radiation introduces random jitter in phase and frequency, resulting in phase-frequency noise that causes the laser linewidth to spread. Therefore, linewidth is an important parameter for characterizing the phase noise of a laser. Combining the relaxation oscillation frequency and damping factor, the Fourier transform of the set of rate equations for the semiconductor laser according to the Wiener-Hinchin theorem gives the following relationship between the frequency noise and the linewidth:

$$S_v(f) = \frac{\delta_{vST}}{\pi}\left[\frac{1+\alpha^2 {f_r}^4}{\left(f^2-{f_r}^2\right)^2 + f^2\frac{\gamma^2}{4\pi^2}}\right], \tag{6}$$

where f_r is the relaxation oscillation frequency, γ is the damping factor, α is the linewidth enhancement factor, and δ_{vST} is the Schawlow–Townes linewidth [21,22] which can be expressed as

$$\delta_{vST} = \frac{v_g{}^2 h\nu n_{sp}(\alpha_m + \alpha_i)\alpha_m}{8\pi P}, \tag{7}$$

where ν_g is the group velocity, $h\nu$ is the photon energy, n_{sp} is the spontaneous radiation factor, α_m is the equivalent mirror loss, α_i is the internal loss, and P is the output power of the laser. The introduction of the linewidth enhancement factor α combined the theoretical and experimental noise of the laser effectively which is defined as

$$\alpha = \frac{\partial n'/\partial N}{\partial n''/\partial N}, \tag{8}$$

where N is the carrier density, n' is the real part of the effective refractive index, and n'' is the imaginary part of the effective refractive index.

The interactions and transitions between photons and carriers caused by stimulated radiation enable the transformation of intensity noise and phase (frequency) noise. Thus, a specific relationship exists between the RIN and the linewidth, which can be expressed as [23,24].

$$R_{RIN(f)} = \frac{4}{\pi}\delta_{vST}\frac{f^2 + (\gamma^*/2\pi)^2}{\left(f_r{}^2 - f^2\right) + f^2(\gamma/2\pi)^2}, \tag{9}$$

where f_r is the relaxation oscillation frequency, γ is the damping factor, γ* is the damping factor considering nonlinear gain compression. Therefore, reducing the RIN is similar to obtaining a narrow linewidth, and a narrow linewidth, high power, and low RIN can usually be obtained simultaneously.

3. Frequency characteristics and measurement methods

3.1. Frequency characteristics of noise in semiconductor lasers

Accurate measurement of the noise of semiconductor lasers establishes a reliable benchmark for studying and analyzing low-noise semiconductor lasers. Understanding the spectral characteristics of semiconductor laser noise is essential for developing appropriate measurement methods for different types of noise, because noise generation mechanisms vary across different frequency ranges.

The noise characteristics of semiconductor lasers vary depending on their frequencies. At low frequencies, 1/f noise dominates, with its PSD adjusting accordingly [25]. In the mid-frequency range, relaxation oscillations can lead to one or more narrow peaks in the noise power spectrum [26,27]. White noise, primarily comprising thermal noise and shot noise, predominates in the high-frequency spectrum. Notably, the PSD demonstrates no significant variation with the frequency. A common occurrence in electronic devices, 1/f noise refers to random fluctuations where the PSD is inversely proportional to frequency. In semiconductor lasers, 1/f noise has two primary sources. One source is the fluctuation in the number of charge carriers in semiconductor devices due to the random capture and emission of carriers by trap centers in regions, such as the space charge region and surface oxide layer. The other component arises from the fluctuation in the mobility of materials or devices caused by the randomness of various scattering processes [28,29]. This noise component exhibits approximately the same intensity for devices with different materials and structures and cannot be fundamentally eliminated. Relaxation oscillations result from the interaction between radiation and the gain medium within the resonant cavity of a laser. Several factors, including the carrier lifetime, injection current ratio, photon lifetime, gain coefficient, and

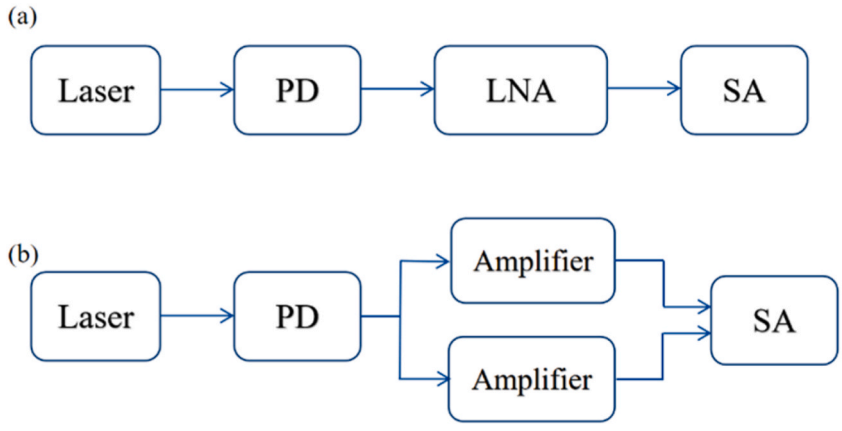

Fig. 1. (**a**) Schematic of the direct measurement method. (**b**) Schematic of cross-spectral measurement.

threshold carrier density, can influence the frequency of relaxation oscillations. White noise, characterized as a random signal or stochastic process with a constant PSD, represents intrinsic noise in semiconductor lasers, primarily thermal and shot noise [30,31]. Thermal noise arises from the random movement of carriers due to thermal excitation, whereas shot noise results from the independent and random passages of the carriers through potential barriers. In the typical frequency range, the power spectral densities of both thermal and shot noise are independent of frequency [32–34]. To achieve accurate RIN measurements, minimizing the influence of interfering noise is necessary. Conducting measurements in the high-frequency range effectively reduces the impact of 1/f noise on RIN measurements.

3.2. RIN measurement methods

Various measurement schemes exist for assessing the RIN of semiconductor lasers; however, the direct measurement method is the most convenient. The measurement principle diagram is shown in Fig. 1 (a). In this approach, the output light undergoes photoelectric conversion, transforming it into a current waveform. Subsequently, the frequency spectrum is directly measured using a spectrum analyzer (SA) after amplification by a low-noise amplifier (LNA). The signal input to the amplifier encompasses both a strong DC signal and weak noise signal owing to the presence of the RIN. Given that the detection target is a fluctuating noise signal, the amplifier must effectively filter out interfering DC signals. Moreover, the amplifier must possess high gain to ensure that the noise signal, post-amplification, is not overshadowed by the inherent noise generated by the SA. Semiconductor lasers typically exhibit weak RIN signals, usually on the order of several tens of nV/$\sqrt{\text{Hz}}$ [35]. Therefore, although measuring RIN through this scheme is relatively convenient, it necessitates using a high-quality amplifier. This amplifier should effectively filter the DC signal and offer substantial gain. The noise floor of the amplifier and susceptibility to power-supply interference can significantly impact measurement results. The minimum effective noise voltage spectrum remains low despite implementing an LNA and shielding measures. In the high-frequency range, the signal received by the SA comprises the RIN, the shot noise power of the photodetector, and the total measured thermal noise power of the receiver, which can be expressed as

$$P_n = P_{n(laser)} + P_{n(shot)} + P_{n(thermal)}, \tag{10}$$

where P_n is the noise power measured by the SA, $P_{n(laser)}$ is the noise power of the laser, $P_{n(shot)}$ is the shot noise power of the photodetector, and $P_{n(thermal)}$ is the total measured thermal noise power of the receiver. When the laser output is deactivated, the thermal noise power spectrum is observable on the SA. Calculating the shot noise entails utilizing the input impedance of the oscilloscope and the DC of the link, which can be expressed as

$$P_{n(shot)} = 2qU, \tag{11}$$

where q is the charge constant and U is the DC voltage. It becomes imperative to eliminate both thermal and shot noise before obtaining the RIN of the laser under testing, which can be expressed as

$$RIN_{(measured)} = RIN_{(laser)} + \frac{2q}{I_{dc}} + \frac{P_{n(thermal)}}{UI_{dc}}, \tag{12}$$

where $RIN_{(measured)}$ is the RIN that was measured, $RIN_{(laser)}$ is the RIN of the laser, and I_{dc} is the DC current in the link.

Nevertheless, the direct measurement method places excessively stringent requirements on the noise characteristics of amplifiers. A more effective approach to overcome these limitations is to adopt the cross-spectral density measurement method as shown in Fig. 1 (b). In this method, the RIN spectrum is measured by connecting two preamplifiers to an SA. Notably, because two separate power sources independently power the amplifiers, the noise introduced by power-supply interference and the noise generated by the amplifiers are independent and uncorrelated. This independence can be exploited through cross-spectral estimation, effectively mitigating the impacts of amplifier noise, zero drift, and other related factors. By employing this method, one can effectively address the effects of amplifier self-noise and power-supply interference on the test results. Consequently, this reduces the requirements placed on the amplifier and ensures a higher level of measurement accuracy.

When measuring the RIN of a laser, the measurement setup often introduces additional noise sources [36]. Among these, 1/f noise predominantly manifests in the low-frequency range, significantly impacting RIN measurements within this frequency band. To enhance the accuracy, the phase noise estimation method shifts the measurement to the high-frequency range. The measurement principle involves modulating the output light of the laser under testing with a single-frequency microwave signal. Due to the inherent noise in the link, the phase noise of the modulated light increases. The phase noise in the measurement link is characterized by the phase noise of the single-frequency point source, total noise power in the link, and output power of the link. The total noise power includes shot noise, thermal noise, and RIN. Intensity noise measurements can be converted into a phase noise measurement. The specific steps in this approach are as follows. First, the single-frequency point microwave signal is connected to the phase noise analyzer to measure the phase noise. Subsequently, the detection link is connected to the modulator, adjusting the modulator bias voltage to operate at the quadrature bias point. The input optical power of the detector and the output optical power of the laser are then measured using an optical power meter, followed by calculating the gain of the link and determining the output photocurrent from the detector response. Finally, the output optical power and phase noise are recorded. The outlined measurement steps show that the phase noise estimation method involves a relatively complex measurement process. Additionally, owing to the susceptibility of the supply voltage of the modulator to environmental disturbances causing drift [37,38], an additional control circuit is necessary to

maintain stability.

The crux of the RIN measurement system lies in the careful selection of low-noise photodetectors and SAs, thoughtful design of signal amplifier circuits, optimization of backend signal acquisition and processing circuits, and refinement of algorithms [39–42]. Among these approaches, the direct measurement method is more practical, whereas the cross-spectrum method requires additional devices and entails computational complexity. Furthermore, currently available commercial amplifiers predominantly operate at high frequencies. Although this choice reduces the power requirements of the amplifier, it does not effectively suppress 1/f noise in the low-frequency range. By contrast, the phase noise estimation method involves excessively complex measurement steps. Consequently, direct measurements are the most widely employed method for practical measurements.

3.3. Measurement methods of phase noise

Although the linewidth can characterize the phase noise of a semiconductor laser, it does not reflect the phase noise characteristics of the laser as a whole. Therefore, the application of lasers is also inseparable from understanding and measuring the phase noise characteristics of lasers. At present, the measurement methods of laser phase noise mainly include direct measurement method, phase discrimination method, frequency discrimination method, coherence method and so on.

The simplest method of measuring phase noise is to directly use an SA. The signal to be measured contains both amplitude noise and phase noise interspersed with the carrier frequency. Therefore, a suitable SA can be used to test the spectral information of the unmodulated signal to be measured. The spectral information appearing on the SA can then be converted into single-sideband phase noise. Although the measurement method is straightforward, the accuracy of the test results may be compromised because of the noise floor of the SA not being sufficiently low. To ensure high-precision measurements, using an SA with a low-noise floor is crucial. Additionally, the measurement results of the SA include both amplitude noise and phase noise in the frequency domain, meaning that the amplitude noise level of the measured signal cannot exceed the phase noise.

Phase discrimination is currently the most widely used measurement method. Most major phase noise test instrument manufacturers use this method in their phase noise test systems. The phase discrimination method aims to convert the phase jitter of the laser being measured into intensity changes using a highly stabilized reference laser as illustrated in Fig. 2 (a) [43]. The phase noise of the laser being measured is then obtained by directly measuring the intensity changes. The process of phase discrimination involves converting the measured signal and reference signal through a phase discriminator and phase-locked loop into a random fluctuation in the phase of the two linear output voltage changes. The output of the phase identification is further processed through a low-pass filter (LPF) and an LNA to facilitate subsequent processing within a certain range of signal frequency and amplitude. The final output signal

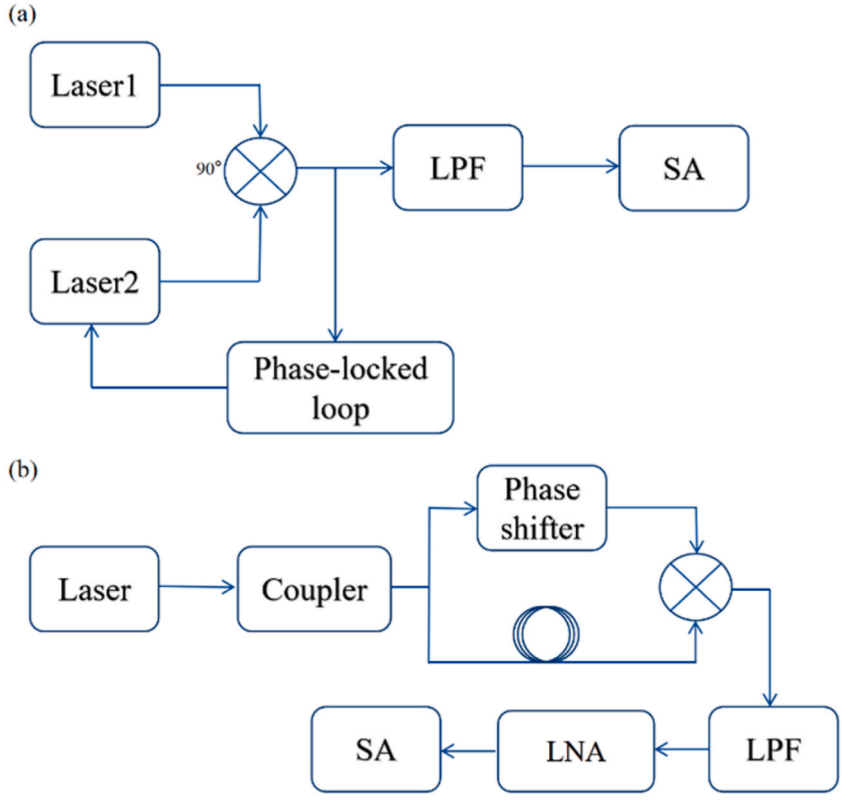

Fig. 2. (**a**) Principle of phase discrimination measurement. (**b**) Principle of frequency discrimination measurement.

is then analyzed directly by the spectrometer. By selecting a suitable reference signal, phase noise measurements based on phase discrimination can achieve very low noise floors, resulting in a robust measurement dynamic range.

To address the limitations of the phase identification method, which requires a high reference source, the frequency discrimination method can be used to measure phase noise. This method uses a discriminator to detect the frequency change of the measured signal, converts the frequency jitter of the laser into phase jitter, and characterizes the phase jitter in the form of intensity change without needing a reference source as shown in Fig. 2 (b) [44,45]. The frequency discrimination method through the power divider involves measuring a frequency signal split into two signals with the same amplitude. One signal passes through a time-delay optical fiber, whereas the other signal travels through a phase shifter. The phase shifter is adjusted until the two signals maintain a phase difference of 90°. Finally, use the phase discriminator on the two orthogonal signals to convert the phase noise into an amplitude and noise proportional to the voltage signal. Before entering the SA, this voltage signal passes through a low-pass filter and a low-noise amplifier, and Fourier transform analysis can then be used to obtain the phase noise power spectrum. This method is easy to implement and does not require a high-precision reference signal. The phase discriminator effectively suppresses amplitude noise, reducing interference with phase noise measurement and enabling high-accuracy measurement of small signals. However, the slope of the discriminator response curve can seriously affect the measurement accuracy. Additionally, the frequency range of the measurement is limited because of the narrow phase discrimination bandwidth of the discriminator.

The methods of discriminating frequency and phase have significant advantages in terms of measurement accuracy compared to the direct measurement method of the SA. However, instantaneous phase change of the laser is still impossible to measure directly. Among the methods for characterizing phase noise, the delayed autocorrelation method only measures a 3 dB line width, which is insufficient for comprehensive characterization. In recent years, researchers have combined the delayed autocorrelation method with phase modulation detection, which is used to determine the differential phase coherently, enabling more complete characterization of the phase noise of the laser [46,47]. The self-external coherent detection method based on phase modulation and the self-zero-difference photocoherent reception method are commonly used. This method recovers an isotropic component I and an orthogonal component Q with phase noise information at the carrier or first harmonic. The FM noise power spectrum and linewidth of the laser are then obtained from the I/Q components in a digital signal processing system. The basic principle of the self-zero-difference optical coherent reception method is to split the laser to be measured into two paths, one as the signal light through the time-delay fiber, and the other directly as the principal oscillator light of the coherent receiver. The role of the coherent receiver is to signal light and local oscillation light for coherent demodulation. It recovers the I/Q component with the laser differential phase noise and obtains the FM noise power spectrum and line width in the digital signal processing system. The coherent detection method employs polarization multiplexing technology in its coherent receiver, significantly increasing the communication capacity. However, self-zero difference coherent detection uses the same frequency for the signal light and the center frequency of the local oscillation light, and the coherent receiver has multiple Mach–Zehnder interferometer (MZI) structures that are highly sensitive to phase changes, making the entire system sensitive to external ambient temperature and vibration, and resulting in poor stability of signal transmission.

Various methods exist for measuring phase noise, each with its advantages, disadvantages, and applications. The direct measurement method using an SA has a larger noise floor but is convenient for engineering tests that do not require high measurement accuracy. The frequency discrimination method is less expensive and can work without a reference source. The phase discrimination method has been continuously improved in recent years, resulting in increased measurement accuracy and decreased constraints. This method is currently one of the most commonly used. The coherent detection method is the most commonly used for phase testing of narrow linewidth lasers owing to its high measurement accuracy, capability for direct measurement of the instantaneous phase change, and low cost of digital signal processing systems.

4. Methods of suppressing noise

As the signal-to-noise ratios of systems continue to improve, the noise characteristics of the light source increasingly limit the performance of lasers. Researchers have attempted to suppress the noise in semiconductor lasers considering various perspectives. Chip structures, selection of materials, external cavity feedback, fabrication processes, and external control circuits can all lead to variations in the noise of semiconductor lasers [48]. This paper focuses on noise reduction from the perspectives of material optimization, structural design, and feedback control.

4.1. Chip structure design

Linewidth and noise reduction in semiconductor lasers can be approached from various angles. From the perspective of epitaxial growth, the linewidth enhancement factor can be reduced and spatial hole burning can be suppressed by increasing the differential gain of quantum wells. These objectives can be achieved by using strained quantum wells and an appropriate increase in their number to reduce the threshold current and enhance the slope efficiency [49–59]. From the perspective of the resonant cavity, increasing the cavity length appropriately can produce a high-quality factor Q, resulting in a narrow linewidth [60–67]. Additionally, applying anti-reflective (AR) coatings on one end of the laser and highly reflective (HR) coatings on the other can improve the stability of the output optical modes and effectively suppress noise [45,46]. For the design of Bragg gratings, high differential gain is obtained by controlling the grating morphology and type, designing suitable grating coupling coefficients, and wavelength blueshift biasing to narrow the linewidth [68–91]. Furthermore, the RIN and phase noise of semiconductor lasers are caused by photon and carrier density fluctuations. Therefore, the waveguide structure of the chip plays a crucial role in determining the distribution of carriers and optical modes. Well-designed waveguide structures, such as buried heterostructures (BHs) and separate confinement heterostructures (SCHs),

can significantly reduce the fluctuations of carrier and photon densities, resulting in effective noise suppression.

The BH structure is a commonly employed solution for high-power, low-noise lasers. The carrier extension in the BH and ridge waveguide (RWG) structures is illustrated in Fig. 3 (a) and 1 (b). The RWG structure exhibits limited restrictions on the injected carriers along the direction parallel to the PN junction. The carrier densities undergo temporal variations with the diffusion and recombination of carriers over time. In contrast, the BH structure introduces a lateral barrier layer in the active region, forming a reverse-biased PN junction. This enhancement improves the blocking capabilities of carriers and photons, limiting the optical field horizontally and vertically. Additionally, the smaller active region area in the BH structure facilitates the acquisition of an active region with minimal or no defects, effectively reducing carrier recombination effects [92–95]. Hence, BH structures have been extensively employed in the research on high-power, low-noise semiconductor lasers. The silicon-based waveguide has the characteristics of small size, high-speed transmission, low loss, and strong compatibility, which is the expected direction of optical chip development. On the one hand, silicon-based external cavity structure is the optimal solution to realize low-noise laser. On the other hand, with the development of heterogeneous integration technology, new structures, such as SI-InP BH, have become the focus of research in recent years [96–98].

In 2003, Takaki et al. developed a 1550 nm DFB laser with an InGaAsP-InP BH structure grown through metal–organic chemical vapor deposition (MOCVD). It exhibited an output power of more than 175 mW, an RIN close to −160 dBc/Hz and a narrow linewidth below 0.8 MHz [99]. The active region of the laser comprised six quantum wells with two end facets coated with AR and HR layers. The resonant cavity was configured as an elongated cavity to attain a higher power. By reducing the carrier densities and optimizing the grating coupling coefficient $\boldsymbol{\kappa}$ within the resonant cavity, the uniformity of the photon densities was improved, resulting in lower noise. Subsequently, Huang et al. employed a BH structure to achieve a DFB laser with an output power of up to 180 mW, a narrow linewidth below 100 kHz, and an RIN below −170 dBc/Hz [100]. The active region of this laser was composed of multiple quantum wells (MQWs) and separate confinement layers (SCHs), forming a mesa structure via wet etching in the active region. The two end facets were coated with AR and HR layers to maintain the excellent single-mode characteristics of the DFB laser, and a grating layer was grown using holographic techniques. In 2011, Zhao et al. employed a BH structure to develop a 1550 nm DFB laser [101], achieving an output power exceeding 200 mW with an RIN below −165 dBc/Hz. The active region of this laser comprised six compressively strained (1 %) quantum wells with a thickness of 6 nm. The quantum wells were sandwiched between the upper and lower SCH layers to confine the carriers horizontally. Additionally, grooves were etched on both sides of the mesa to further enhance the carrier confinement. The cavity length of the laser was set between 1.5 mm and 2.0 mm to achieve high output power. The optimal $\boldsymbol{\kappa}$ value was determined to satisfy the condition $\boldsymbol{\kappa}L = 1.25$ [102], effectively suppressing spatial hole burning. In 2014, Feng et al. reported a DFB laser with a BH structure, featuring a central wavelength of 1310 nm, an output power of up to 207 mW, and an RIN below −160 dBc/Hz within the 1–30 GHz range [103]. This DFB laser utilized six pairs of undoped InGaAsP quantum wells, with both the upper and lower SCH layers employing four different bandgap structures. The cavity length was set between 1.3 and 2.0 mm, with a selected cavity length of 1.4 mm to achieve high output power, and $\boldsymbol{\kappa}L$ was designed to be 1.05. In 2021, Wu et al. achieved a 1550 nm DFB laser with a BH structure, demonstrating an output power exceeding 102 mW at room temperature and an RIN lower than −160 dBc/Hz [92]. The laser output power was enhanced through mutual matching of the cavity length and quantum wells, along with the optimized design of the optical waveguide. A partial grating structure was implemented to suppress the spatial hole-burning effect. In 2024, Guo et al. reported a single-mode InGaAsP/InP BH lasers based on high-order slotted surface grating, featuring a central wavelength of 1563 nm, an output power of 10.2 mW, and a narrow linewidth of 550 kHz [104]. Addition, the structures of SI-InP BH have also been widely used in recent years. In 2018, Shinji et al. fabricated membrane BH lasers on SiO_2/Si substrates through the combination of direct bonding and epitaxial growth [96]. In 2020, Takuro et al. reported the direct modulation of membrane BH lasers on silicon. The MQW layer, sandwiched between InP layers, is directly bonded to a Si substrate with thermal oxide (SiO_2/Si substrate) [97]. In the same year, Takuma et al. reported bonding an InP substrate containing the MQWs to a Si substrate containing the Si waveguide circuits. The cores

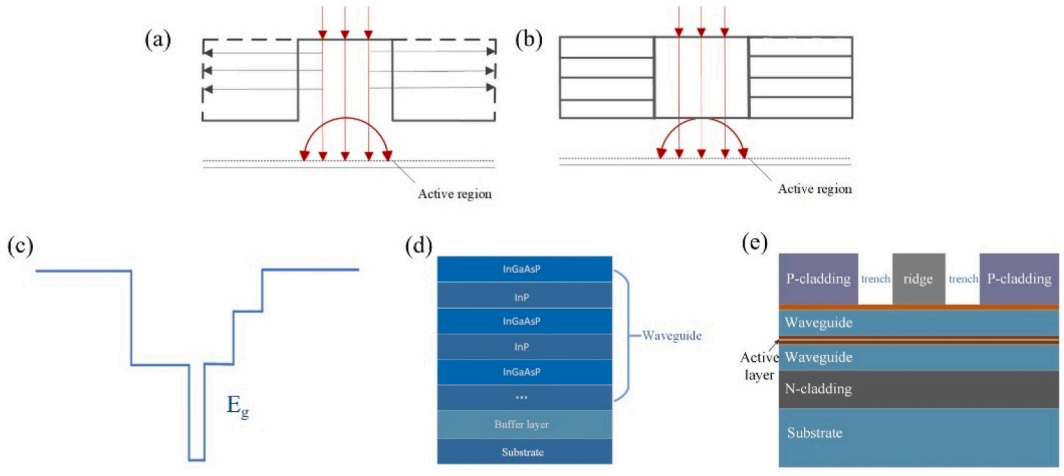

Fig. 3. (**a**) Carrier extension in RWG. (**b**) Carrier extension in BH structure. (**c**) Energy map of the conduction band of the asymmetric SCH structure. (**d**) Dilute waveguide epitaxial distribution. (**e**) Schematic of the structure of a double-trench ridge waveguide.

of the MQW layer and bulk layer are etched, after which the InP is regrown to create BHs [98].

Although the BH configuration offers numerous advantages for enhancing laser output performance, its fabrication process is intricate. Several research institutions have recently explored asymmetric cladding structures to mitigate the noise. These include configurations with asymmetric SCH, diluted waveguide structures, and dual-groove ridge waveguide structures. Unlike symmetric SCH, asymmetric SCH integrates high-bandgap materials in a p-type confinement layer to mitigate carrier leakage. The conduction band energy distribution of the asymmetric SCH structure is shown in Fig. 3 (c). The asymmetric distribution of the refractive index causes the optical field to deviate from the p-type material side with a high absorption loss, directing more light into the n-type material. This reduces the optical absorption loss of carriers and effectively suppresses the noise. The diluted waveguide was constructed from multiple periodically arranged non-doped InP/InGaAsP composite layers, as shown in Fig. 3 (d). The refractive-index distribution is controlled by designing the period and thickness, guiding the optical field to low-loss layers, and effectively suppressing the noise. Compared with the ridge waveguide, the double-trench ridge waveguide provides enhanced confinement for carriers and photons. The schematic diagram of the structure of a double-trench ridge waveguide is shown in Fig. 3 (e). In a ridge-type waveguide, isotropic confinement along the p-n junction plane leads to ineffective carrier confinement and carrier spreading. Introducing a double-trench structure increases the refractive-index difference in the external structure, effectively confining carriers and photons within the emitting region [105]. Additionally, the introduced passive lower waveguide weakens the lateral light confinement of the ridge waveguide, reducing the photon absorption caused by the p-doping layer and further lowering the noise [106].

In 2011, Faugeron et al. utilized gas-source molecular beam epitaxy (GS-MBE) to grow an MQW DFB structure on an N-InP substrate. The double-trench ridge waveguide was fabricated through ion beam etching, wet chemical etching, and proton isolation, yielding a 1550 nm DFB laser with an output power of up to 140 mW and RIN below −157 dBc/Hz in the range of 0.1–20 GHz [107]. This structure reduces the optical overlap between the optical intrinsic mode and the p-doping layer, thereby decreasing the optical confinement factors associated with quantum wells. To counteract this effect, the number of quantum wells in the active region was increased to prevent an increase in the detrimental threshold current. In 2012, Faugeron et al. reported a 1550 nm DFB laser based on a diluted waveguide [108]. The chip achieved an output power of approximately 180 mW at temperatures ranging from 15 to 85 °C. Within the frequency range of 0.08–40 GHz, the optical linewidth was less than 300 kHz and the RIN remained below −160 dBc/Hz. The diluted waveguide consisted of 15 InGaAsP/InP layers and was positioned below the MQW. Subsequently, Wang et al. reported a semiconductor laser with a central wavelength of 1550 nm, capable of achieving an output power exceeding 140 mW, a narrowest linewidth of 520 kHz, and an RIN below −145 dBc/Hz [109]. They utilized an AlGaInAs material system with favorable temperature characteristics and high differential gain as the quantum wells and waveguide layers, respectively, to achieve a high output power. The growth technique utilized was MOCVD on an N-InP substrate with three pairs of alternately grown diluted waveguides designed to minimize internal losses within the active region. Implementing a graded-index separate confinement heterostructure was crucial for reducing carrier leakage and enhancing the internal quantum efficiency. Furthermore, a suspended grating structure was strategically employed, enabling precise control over the physical characteristics of the grating. In 2022, Liu et al. introduced a high-power continuous-wave (CW) DFB laser based on an AlGaInAs MQW operating at a central wavelength of approximately 1310 nm [110]. This laser achieved a remarkable room-temperature output power exceeding 173 mW, accompanied by an RIN below −155 dBc/Hz and a Lorentz linewidth less than 600 kHz. The laser featured a double-trench ridge waveguide structure incorporating a strategically placed InGaAsP far-field reduction layer below the MQW in the active region. This design optimization aims to shift the optical mode field towards the n-type cladding layer, effectively reducing the far-field divergence angle and simultaneously lowering the optical confinement factor of the quantum-well region and overall optical absorption losses. In the same year, Xiang et al. developed a 1550 nm DFB laser with an output power exceeding 170 mW, a narrow linewidth of 250 kHz and a low RIN below −157 dBc/Hz [111]. This laser employed a double-waveguide structure by introducing a low-optical-confinement-factor InP layer below the active region and a 300-nm-thick lightly doped N-type InGaAsP passive waveguide layer. This innovative design aimed to reduce the overlap between the optical mode and the p-type doping layer. In addition, a quarter-wavelength phase shift was introduced into the grating to achieve a single-longitudinal mode output. The coupling coefficient κL was designed to be approximately 1 to mitigate the spatial hole-burning effects.

Both the BH structure and asymmetric cladding structures are successful in suppressing noise, but the BH structure provides a more stable mode output. Table 1 shows that Emcore Corporation utilized BH structure to reduce RIN to −170 dBc/Hz and narrow the

Table 1
Comparison of schemes and indices of different semiconductor lasers.

Year	Research institution	Scheme	RIN	Linewidth	Output power
2003	Furukawa Electric	BH	−160 dBc/Hz	0.8 MHz	175 mW
2010	Emcore Corporation	BH	−170 dBc/Hz	100 kHz	180 mW
2011	Apic Corporation	BH	−165 dBc/Hz	/	200 mW
2011	Thales Air Systems	Double-trench ridge waveguide	−157 dBc/Hz	/	140 mW
2012	Thales Air Systems	Diluted waveguide	−160 dBc/Hz	300 kHz	180 mW
2014	COE	BH, SCH	−160 dBc/Hz	/	207 mW
2019	CAS	Diluted waveguides	−145 dBc/Hz	520 kHz	140 mW
2021	CETC	BH	−160 dBc/Hz	/	102 mW
2022	CAS	Double-trench ridge waveguide	−155 dBc/Hz	600 kHz	173 mW
2022	HUST	Double-trench ridge waveguide	−157 dBc/Hz	250 kHz	170 mW
2024	CAS	BH	/	550 kHz	10.2 mW

linewidth to 100 kHz, which is the best level achieved thus far using internal cavity technology. However, the BH structure involves selective regional growth, complicating material growth and manufacturing process. The precise control of doping concentration is crucial, as its optimization can enhance the differential quantum efficiency. However, excessively high doping concentration may introduce defects and stresses, thereby increasing noise levels. Therefore, the design of epitaxial layers and optical waveguide structures must consider both the output characteristics of the laser and the manufacturing processes.

4.2. External cavity structure

High-power, low-noise semiconductor lasers with intracavity feedback typically integrate Bragg gratings or specific waveguide structures within the active cavity. However, a long cavity causes significant optical losses, which limit the laser power, making it challenging to achieve high output power and low noise simultaneously. In 1980, Lang and Kobayashi proposed external cavity feedback semiconductor lasers [112]. External cavity feedback technology has quickly become a research focus, and external cavity structures have gradually become the primary structures for obtaining high-power, low-noise semiconductor lasers. The most commonly used method is injection locking.

The injection locking technique has been widely applied in research on narrow-linewidth semiconductor lasers [113,114]. After Adler derived basic equations to describe oscillator injection locking in 1946 [115], Paciorek provided differential equations to describe injection locking with a strong signal based on Adler's theory [116]. Subsequently, Kurokawa conducted analyses of injection locking, including the locking bandwidth, locking stability, frequency of the locking process, and amplitude noise [117]. Depending on the source of the injected light, injection locking can be classified into master–slave locking and self-injection locking. The fundamental principle of master–slave injection locking involves injecting an optical signal from an external master laser into a slave laser. When the injected wavelength falls within the locking range of the injected laser, the output frequency is locked to the frequency of the externally injected laser, and consequently, the free oscillation mode is suppressed. External light injection reduces the concentration of free carriers in the active region of the laser. As the injection power gradually increases, the carriers within the cavity are depleted, and their concentrations falls below the threshold. This prompts the injection-locked laser to reach single-mode oscillation, with carriers being consumed steadily, suppressing the noise. Master–slave injection locking requires the frequencies of the master and slave lasers to be appropriately closed, including the two lasers in the system. This increases complexity during the setup, as well as its scale and expense. Currently, external cavity feedback self-injection locking is often used to suppress the noise in high-power, low-noise semiconductor lasers. The theoretical model for this system was proposed by Lang and Kobayashi [118], and its structural diagram is shown in Fig. 4. External cavity feedback self-injection locking typically involves the use of optical feedback components, such as fiber Bragg gratings (FBGs), whispering-gallery-mode resonators (WGMRs), and planar waveguides added externally to the laser to achieve specific wavelength selection. This procedure is achieved by filtering the frequency of the optical signal through the external cavity before injecting the feedback light back into the laser, inducing further stimulated emission. Consequently, priority is given to the longitudinal mode that undergoes this process, resulting in earlier saturation of mode competition and suppression of other modes. The gain in the feedback mode is increased. This mechanism stabilizes the consumption of carriers during competition between modes.

In 2010, Liang et al. started systematically exploring external cavity feedback self-injection locking, focusing on a WGMR with an ultrahigh quality factor. In the initial stages, GaF_2 microresonators were employed, accomplishing a linewidth reduction in the DFB semiconductor laser to 200 Hz while maintaining high-frequency stability with phase noise as low as −125 dBc/Hz [119]. In 2015, they used a WGMR composed of MgF_2 as an external cavity for feedback [120]. The experimental setup is shown in Fig. 5 (a). The laser frequency noise achieved is on the order of 0.3 $Hz/Hz^{1/2}$ above 10 kHz, featuring 30 Hz integral linewidth as well as sub-hertz instantaneous linewidth. The experimental findings indicated that the laser had an ultralow-frequency noise and an extremely narrow instantaneous linewidth. In 2018, Liang et al. employed a high-Q WGMR as an external feedback cavity to fabricate the semiconductor laser module shown in Fig. 5 (b). The module operated at high power and low noise, with a central wavelength of 1550 nm, an output power exceeding 110 mW, an RIN lower than −160 dBc/Hz, a linewidth less than 100 Hz, and a frequency noise of 1

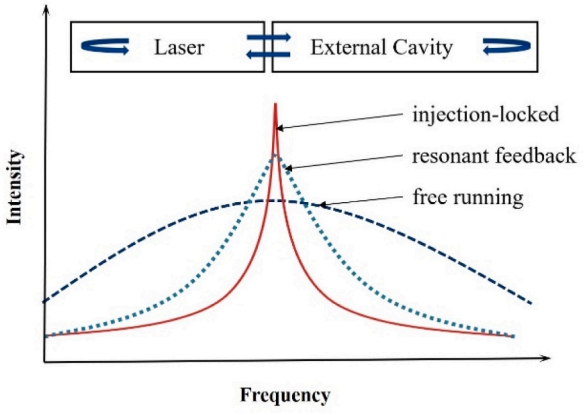

Fig. 4. Schematic of self-injection locking.

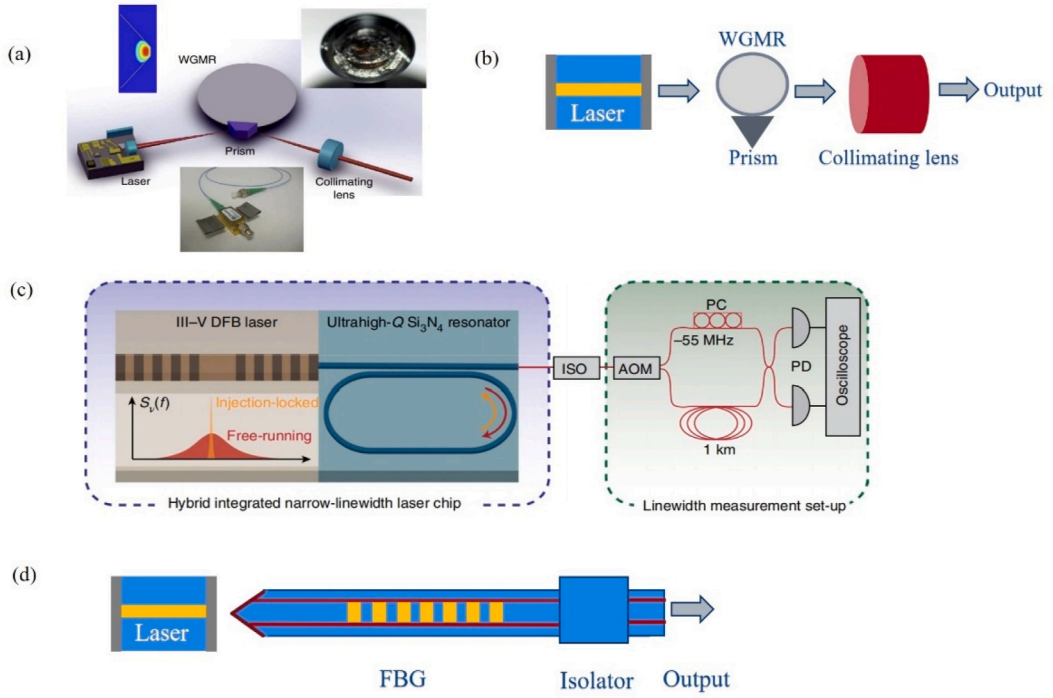

Fig. 5. (a) Schematic of the experimental setup. (b) Schematic of the module. (c) Schematic of the slab-coupled optical waveguide external cavity laser. (d) Structure diagram of the hybrid integrated semiconductor laser.

Hz/Hz$^{1/2}$ at 100 kHz frequency offset [121]. The DFB laser emitted light in this module, focusing on the WGMR using an evanescent field coupling mirror. The light emitted from the prism was directed toward a booster semiconductor optical amplifier (SOA) operating in a saturated state. An optical isolator was positioned between the amplifier and the WGMR to prevent any light from the amplifier from feeding back into the WGMR. The external cavity optical feedback method, grounded in WGMR, can produce a laser output characterized by ultralow noise and a narrow linewidth. However, this method requires resonators with exceedingly high Q values and the coordination of intricate coupling devices, irrespective of whether optical fiber or nonfiber components are used. This intricacy presents challenges for system adjustment. In 2021, Jin et al. reported an ultra-narrow linewidth semiconductor laser using an ultra-high-Q Si_3N_4 microresonator. The schematic of the laser design is shown in Fig. 5 (c). The team reduced the noise by self-injection-locking a conventional DFB laser to ultra-high-Q microresonators yielding a frequency noise of 0.2Hz2Hz−1, with a corresponding short-term linewidth of 1.2 Hz and an output power up to 30 mW [122]. In 2022, Takuma et al. presented a tunable laser composed of a Si lattice filter serving as the cascaded-delay interferometer, a Si ring resonator, and a III-V gain region. They employed epitaxial growth to create an InP layer, which was then directly bonded onto a Si photonics wafer to form a BH for the III-V gain region. Photolithographic markers were utilized on a Si layer to precisely define the position of the BH. The laser on a silicon photonics platform demonstrates a Lorentzian linewidth of less than 40 kHz [123]. In 2023, Chen et al. designed and fabricated a hybrid integrated laser with narrow linewidth and high-power output [124]. The external cavity laser is composed of a gain chip and a dual micro-ring narrowband filter integrated into the silicon nitride photonic chip achieving an output power of 220 mW and linewidth narrower than 8 kHz over the full C-band. In 2023, Xiang et al. presented an ultralow-noise isolator-free laser by using three-dimensional laser integration with ultralow-loss (ULL) technologies. By employing multiple monolithic and heterogeneous processing sequences, they have successfully demonstrated the direct on-chip integration of III–V gain medium and ULL silicon nitride waveguides. The white noise floor for the drop port is 1.7 Hz2 Hz−1, indicating a fundamental linewidth of about 5 Hz [125].

When employing an FBG as the feedback external cavity, fusion splicing is utilized between the gain chip and the FBG with a lensed fiber, eliminating the need for intricate optical path adjustments. This approach has several benefits, including low cost, compact structure, excellent stability, and high coupling efficiency. It is common practice to incorporate an optical isolator after the fiber Bragg grating to reduce backward reflections within the cavity. Furthermore, with the continuous development of semiconductor gain chip technology and FBG writing processes, the performance of semiconductor gain chips and design flexibility of the grating spectrum have significantly improved. In recent years, fiber Bragg-grating-based external cavity semiconductor lasers have attracted the attention of research institutions worldwide. Juodawlkis et al. developed a slab-coupled optical waveguide external cavity laser [126]. As shown in Fig. 5 (d), this laser comprised a double-bend channel InGaAlAs quantum-well slab-coupled optical waveguide amplifier (SCOWA) and an external cavity with a narrow bandwidth (2.5 GHz) FBG at a central wavelength of 1550 nm connected through a lensed optical fiber fusion splice. Optical isolators were incorporated downstream from the fiber Bragg grating to minimize backward reflections. Tests were conducted using FBGs with reflectivity I values of 10 % and 20 %, and the RIN values were measured to be as low as −155

dBc/Hz and −165 dBc/Hz, with Lorentz linewidths of 15 kHz and 6 kHz, respectively, for output powers exceeding 400 mW. In 2011, Loh et al. developed a high-power, low-noise external cavity laser based on an InGaAlAs/InP quantum-well structure [127]. This laser integrated a double-bend channel SCOWA with a narrow-bandwidth FBG external cavity through a lensed optical fiber coupling. At an injection current of 4 A, the laser achieved an output power exceeding 370 mW, with an RIN below −160 dBc/Hz and a narrow Lorentz linewidth of 1.75 kHz. In 2018, Morton and Morton achieved a remarkably low noise by employing an FBG as an external feedback cavity [128]. The gain chip featured an AR coating on the output facet and an HR coating on the opposite side. The output was coupled to an external fiber cavity using a lensed optical fiber. The external fiber cavity included an FBG that provided external feedback for self-injection. The FBG was designed to have a relatively short length while minimizing the sizes of the side modes, enhancing the single-mode operation range and stability of the laser, and ultimately reducing the noise. The laser had an RIN as low as −165 dBc/Hz, a Lorentz of 15 Hz, and a frequency noise as low as 4.5 $Hz/Hz^{1/2}$. In 2019, Sun et al. presented a high-power, low-noise hybrid integrated external cavity semiconductor laser operating in the 1550 nm wavelength range [129]. They combined a single-angle facet gain chip and a polarization-maintaining single-mode fiber Bragg grating in the external cavity. The laser polarization output was achieved through coupling with a lensed optical fiber and a polarization-maintaining single-mode fiber Bragg grating. Leveraging the prominent group delay characteristics at the inclined side of the fiber Bragg grating effectively suppressed the noise in the semiconductor laser, yielding an output power exceeding 30 mW, an RIN below −155 dBc/Hz, and a narrow Lorentz linewidth of 1.75 kHz. In 2022, Chen et al. presented a single polarization narrow linewidth hybrid laser with an InP-based gain chip and an external silica-on-silicon (SoS) waveguide Bragg grating (WBG). The laser achieved an output power of 6.53 mW, with an RIN below −158 dBc/Hz and a narrow Lorentz linewidth of 4.35 kHz [130].

Table 2 demonstrates that external cavity feedback is effective for both reducing both the linewidth and RIN. Compared to the internal feedback technique, external feedback is more effective in reducing the linewidth and obtaining higher output power. The design and manufacturing of high-Q external cavities are critical to achieving low noise levels. However, the size constraints of the external cavity make it unfavorable for integration. In the external feedback configurations mentioned earlier, the FBG structure is bulky and poses a challenge in achieving high Q. In contrast, micro-loops are more conducive to achieving high Q [131], thus providing excellent noise rejection. The smaller size also facilitates the achievement of compact and small modules. Nevertheless, challenges arise because of the complexities of coupling and the sensitivity to temperature variations [132].

5. Summary and prospect

In response to increasing demands for accuracy in various applications, particularly in fields, such as optical communication and microwave photonics, where stringent signal-to-noise ratio requirements prevail, the significance of low-noise semiconductor lasers has increased. These lasers play a pivotal role in determining whether a system can meet the practical application requirements of precision-demanding technologies, such as fiber-optic hydrophones and gyroscopes [133–135]. This paper investigates noise measurement and suppression methods for semiconductor lasers, comparing methods of measuring the RIN and phase noise of semiconductor lasers and examining specific suppression strategies employed by research institutions in the development of high-power, low-noise semiconductor lasers. Among the RIN measurement methods, the direct measurement method is widely preferred in practical applications because of its ability to avoid the complex calculations associated with cross-spectrum measurements as well as the intricate measurement steps in the phase noise estimation method. Among the phase noise measurement methods, the phase discrimination method and the coherent detection method have a wide range of measurement bandwidths and are widely used in research and applications. In chip structure design, emphasis is placed on epitaxial layer distributions and waveguide structures, including the BH structure and the asymmetric cladding structure. The BH structure and asymmetric cladding prove effective in noise suppression, although with certain limitations. The BH structure faces challenges in fabrication and necessitates an improved yield, whereas the design of asymmetric claddings encounters difficulties in controlling thickness and doping accuracy, limiting its efficacy in noise suppression. For external cavity structure design, several commonly used external cavity structures are introduced and analyzed,

Table 2
Comparison of schemes and indices of different external cavity diode lasers.

Year	Research institution	Scheme	RIN	Linewidth	Output power
2010	Oewaves	WGMR	/	200 Hz	/
2010	MIT Laboratory	FBG, SCOWA	−165 dBc/Hz	6 kHz	400 mW
2011	MIT Laboratory	FBG, SCOWA	−160 dBc/Hz	1.75 kHz	370 mW
2015	Oewaves	WGMR	/	30 Hz	10 mW
2018	Oewaves	WGMR, SOA	−160 dBc/Hz	100 Hz	110 mW
2018	Morton Photonics	FBG	−165 dBc/Hz	15 Hz	100 mW
2019	SIOM	FBG	−155 dBc/Hz	1.75 kHz	30 mW
2021	UCSB	WGMR, Si_3N_4	/	1.2 Hz	30 mW
2022	CIOMP	SoS, WBG	−158 dBc/Hz	4.35 kHz	6.53 mW
2022	NTTDTL	WGMR, Si	/	40 kHz	/
2023	SIOM	WGMR, Si_3N_4	/	8 kHz	220 mW
2023	UCSB	SiN ring, ULL	/	5 Hz	/

among which micro-rings are more conducive to achieving high Q values than other structures, offering superior RIN suppression effects. However, micro-rings present challenges related to coupling difficulties and sensitivity to temperature variations.

Advanced fabrication processes are prerequisites for the production of high-power, low-noise semiconductor lasers [136–143], and the structural design of lasers must take into account the current level of fabrication. In chip structure design, active region materials can be further optimized and new epitaxial and waveguide structures can be designed to achieve low noise [144,145]. In the field of external cavity feedback technology, continuous innovations in optical feedback elements and external cavity design are crucial for further noise suppression. Intracavity feedback requires a simpler structure and is easier to integrate compared to external cavity feedback. However, the optical loss in the cavity limits the output power of the laser, and high output power and low noise can be simultaneously achieved via a combination of inner- and outer-cavity feedback. Simultaneously, lower noise levels place more stringent requirements on the measurement system. With the development of components and equipment, future noise measurement methods will aim towards simpler test steps and higher measurement accuracy. By contrast, with the rapid development of high-speed optical interconnects and photonic integration chips, the light source is also expected to have smaller sizes to facilitate on-chip integration. Overall, the process of developing low-noise, narrow-linewidth semiconductor lasers include design, characterization, and application, and it is essential that comprehensive development meets the future needs of scientific, technological, and industrial research.

Funding

This research was funded by the National Key R & D Program of China, grant number 2022YFB2803500; the National Natural Science Foundation of China, grant numbers 62090050, 62121005, 61934003, 62227819, and 62090051.

Data availability statement

Data availability is not applicable to this article as no new data were created or analyzed in this study.

CRediT authorship contribution statement

Hua Wang: Writing – original draft, Conceptualization. **Yuxin Lei:** Writing – review & editing, Funding acquisition, Conceptualization. **Qiang Cui:** Visualization, Methodology. **Siqi Li:** Software, Project administration. **Xin Song:** Validation. **Yongyi Chen:** Validation. **Lei Liang:** Validation. **Peng Jia:** Formal analysis. **Cheng Qiu:** Investigation. **Yue Song:** Resources. **Yubing Wang:** Data curation. **Yiran Hu:** Data curation. **Li Qin:** Supervision. **Lijun Wang:** Supervision.

Declaration of competing interest

The authors declare that they have no known competing financial interests or personal relationships that could have appeared to influence the work reported in this paper.

References

[1] N.S. Kopeika, J. Bordogna, Background noise in optical communication systems, Proc. IEEE 58 (1970) 1571–1577, https://doi.org/10.1109/PROC.1970.7982.
[2] N.G. Pavlov, S. Koptyaev, G.V. Lihachev, A.S. Voloshin, A.S. Gorodnitskiy, M.V. Ryabko, S.V. Polonsky, M.L. Gorodetsky, Narrow-linewidth lasing and soliton Kerr microcombs with ordinary laser diodes, Nat. Photonics 12 (2018) 694–698, https://doi.org/10.1038/s41566-018-0277-2.
[3] S.L.I. Olsson, H. Eliasson, E. Astra, M. Karlsson, P.A. Andrekson, Long-haul optical transmission link using low-noise phase-sensitive amplifiers, Nat. Commun. 9 (2018) 2513, https://doi.org/10.1038/s41467-018-04956-5.
[4] M.E. Marhic, P.A. Andrekson, P. Petropoulos, S. Radic, C. Peucheret, M. Jazayerifar, Fiber optical parametric amplifiers in optical communication systems, Laser Photon. Rev. 9 (2015) 50–74, https://doi.org/10.1002/lpor.201400087.
[5] H. He, L. Jiang, Y. Pan, A. Yi, X. Zou, W. Pan, A.E. Willner, X. Fan, Z. He, L. Yan, Integrated sensing and communication in an optical fibre, Light Sci. Appl. 12 (2023) 25, https://doi.org/10.1038/s41377-022-01067-1.
[6] E.A. Kittlaus, D. Eliyahu, S. Ganji, S. Williams, A.B. Matsko, K.B. Cooper, S. Forouhar, A low-noise photonic heterodyne synthesizer and its application to millimeter-wave radar, Nat. Commun. 12 (2021) 4397, https://doi.org/10.1038/s41467-021-24637-0.
[7] X. Luo, X.Y. Han, Y.Y. Gu, S. Li, M. Zhao, Phase noise floor suppression of the output carrier from double sideband-carrier suppressed modulation system, Sci. China Inf. Sci. 54 (2011) 1312–1320, https://doi.org/10.1007/s11432-011-4184-0.
[8] J. Yao, J. Capmany, Microwave photonics, Sci. China Inf. Sci. 65 (2022) 221401, https://doi.org/10.1007/s11432-021-3524-0.
[9] W. Jiang, F.M. Mayor, S. Malik, R. Van Laer, T.P. McKenna, R.N. Patel, J.D. Witmer, A.H. Safavi-Naeini, Optically heralded microwave photon addition, Nat. Phys. 19 (2023) 1423–1428, https://doi.org/10.1038/s41567-023-02129-w.
[10] X. Zhang, Z. Feng, D. Marpaung, E.N. Fokoua, H. Sakr, J.R. Hayes, F. Poletti, D.J. Richardson, R. Slavík, Low-loss microwave photonics links using hollow core fibres, Light Sci. Appl. 11 (2022) 213, https://doi.org/10.1038/s41377-022-00908-3.
[11] M. Jin, S.J. Tang, J.H. Chen, X.C. Yu, H. Shu, Y. Tao, A.K. Chen, Q. Gong, X. Wang, Y.F. Xiao, 1/f-noise-free optical sensing with an integrated heterodyne interferometer, Nat. Commun. 12 (2021) 1973, https://doi.org/10.1038/s41467-021-22271-4.
[12] G. Frascella, S. Agne, F.Y. Khalili, M.V. Chekhova, Overcoming detection loss and noise in squeezing-based optical sensing, npj Quantum Inf. 7 (2021) 72, https://doi.org/10.1038/s41534-021-00407-0.
[13] D. Suess, A. Bachleitner-Hofmann, A. Satz, H. Weitensfelder, C. Vogler, F. Bruckner, C. Abert, K. Prügl, J. Zimmer, C. Huber, S. Luber, W. Raberg, T. Schrefl, H. Brückl, Topologically protected vortex structures for low-noise magnetic sensors with high linear range, Nat. Electron. 1 (2018) 362–370, https://doi.org/10.1038/s41928-018-0084-2.
[14] M. Xu, X. Jia, M. Pickering, S. Jia, Thin cloud removal from optical remote sensing images using the noise-adjusted principal components transform, ISPRS J. Photogramm. 149 (2019) 215–225, https://doi.org/10.1016/j.isprsjprs.2019.01.025.

[15] J. Li, M. Zhang, Physics and applications of Raman distributed optical fiber sensing, Light Sci. Appl. 11 (2022) 128, https://doi.org/10.1038/s41377-022-00811-x.
[16] T. Kessler, C. Hagemann, C. Grebing, T. Legero, U. Sterr, F. Riehle, M.J. Martin, L. Chen, J. Ye, A sub-40-mHz-linewidth laser based on a silicon single-crystal optical cavity, Nat. Photonics 6 (2012) 687–692, https://doi.org/10.1038/nphoton.2012.217.
[17] X. Xie, R. Bouchand, D. Nicolodi, M. Giunta, W. Hänsel, M. Lezius, A. Joshi, S. Datta, C. Alexandre, M. Lours, P. Tremblin, G. Santarelli, R. Holzwarth, Y. Le Coq, Photonic microwave signals with zeptosecond-level absolute timing noise, Nat. Photonics 11 (2017) 44–47, https://doi.org/10.1038/nphoton.2016.215.
[18] R. Gao, J. Park, X. Hu, S. Yang, K. Cho, Reflective noise filtering of large-scale point cloud using multi-position LiDAR sensing data, Remote Sens 13 (2021) 3058, https://doi.org/10.3390/rs13163058.
[19] M. Yamada, Variation of intensity noise and frequency noise with the spontaneous emission factor in semiconductor lasers, IEEE J. Quantum Electron. 30 (1994) 1511–1519, https://doi.org/10.1109/3.299482.
[20] X. Audier, S. Heuke, P. Volz, I. Rimke, H. Rigneault, Noise in stimulated Raman scattering measurement: from basics to practice, APL Photonics 5 (2020), https://doi.org/10.1063/1.5129212.
[21] A.L. Schawlow, C.H. Townes, Infrared and optical masers, Phys. Rev. 112 (1958) 1940–1949, https://doi.org/10.1103/PhysRev.112.1940.
[22] M.W. Fleming, A. Mooradian, Fundamental line broadening of single-mode (GaAl)As diode lasers, Appl. Phys. Lett. 38 (1981) 511–513, https://doi.org/10.1063/1.92434.
[23] N. Yokouchi, N. Yamanaka, N. Iwai, Y. Nakahira, A. Kasukawa, Tensile-strained GaInAsP-InP quantum-well lasers emitting at 1.3 μm, IEEE J. Quantum Electron. 32 (1996) 2148–2155, https://doi.org/10.1109/3.544762.
[24] K. Kikuchi, T. Okoshi, Measurement of FM noise, AM noise, and field spectra of 1.3 μm InGaAsP DFB lasers and determination of the linewidth enhancement factor, IEEE J. Quantum Electron. 21 (1985) 1814–1818, https://doi.org/10.1109/JQE.1985.1072575.
[25] A.A. Balandin, Low-frequency 1/f noise in graphene devices, Nat. Nanotechnol. 8 (2013) 549–555, https://doi.org/10.1038/nnano.2013.144.
[26] C.B. Su, J. Schlafer, R.B. Lauer, Explanation of low-frequency relative intensity noise in semiconductor lasers, Appl. Phys. Lett. 57 (1990) 849–851, https://doi.org/10.1063/1.103385.
[27] D.M. Kane, J.P. Toomey, Precision threshold current measurement for semiconductor lasers based on relaxation oscillation XXX requency, J. Lightwave Technol. 27 (2009) 2949–2952, https://doi.org/10.1109/JLT.2009.2019112.
[28] A.L.Mc Whorter, Semiconductor Surface Physics, University of Pennsylrnia Press, 1976.
[29] A. Van Der Ziel, Noise in solid-state devices and lasers, Proc. IEEE 58 (1970) 1178–1206, https://doi.org/10.1109/PROC.1970.7896.
[30] H.E. Van den Brom, J.M. Van Ruitenbeek, Quantum suppression of shot noise in atom-size metallic contacts, Phys. Rev. Lett. 82 (1999) 1526–1529, https://doi.org/10.1103/PhysRevLett.82.1526.
[31] A. Kumar, L. Saminadayar, D.C. Glattli, Y. Jin, B. Etienne, Experimental test of the quantum shot noise reduction theory, Phys. Rev. Lett. 76 (1996) 2778–2781, https://doi.org/10.1103/PhysRevLett.76.2778.
[32] Y.M. Blanter, M. Büttiker, Shot noise in mesoscopic conductors, Phys. Rep. 336 (2000) 1–166, https://doi.org/10.1016/S0370-1573(99)00123-4.
[33] S. Gozem, I. Schapiro, N. Ferré, M. Olivucci, The molecular mechanism of thermal noise in rod photoreceptors, Science 337 (2012) 1225–1228, https://doi.org/10.1126/science.1220461.
[34] Y.M. Blanter, M. Büttiker, Shot noise in mesoscopic conductors, Phys. Rep. 336 (2000) 1–166, https://doi.org/10.1016/S0370-1573(99)00123-4.
[35] G.A. Cranch, Frequency noise reduction in erbium doped fibre Bragg grating lasers using active electronic feedback, in: 2002 15th Optical Fiber Sensors Conference Technical Digest, USA, Portland, Oregon, 2002, pp. 293–296, https://doi.org/10.1109/OFS.2002.1000560.
[36] K. Haneda, M. Yoshida, H. Yokoyama, Y. Ogawa, M. Nakazawa, Measurements of longitudinal linewidth and relative intensity noise in ultrahigh-speed mode-locked semiconductor lasers, Electron. Comm. Jpn Pt II. 89 (2006) 28–36, https://doi.org/10.1002/ecjb.20185.
[37] H.T. Chen, W.J. Padilla, M.J. Cich, A.K. Azad, R.D. Averitt, A.J. Taylor, A metamaterial solid-state terahertz phase modulator, Nat. Photonics 3 (2009) 148–151, https://doi.org/10.1038/nphoton.2009.3.
[38] T. Alvarez-Segura, J.R. Torres-Lapasió, C. Ortiz-Bolsico, M.C. García-Alvarez-Coque, Stationary phase modulation in liquid chromatography through the serial coupling of columns: a review, Anal. Chim. Acta 923 (2016) 1–23, https://doi.org/10.1016/j.aca.2016.03.040.
[39] E. Rubiola, K. Volyanskiy, L. Larger, Measurement of the laser relative intensity noise, in: 2009 IEEE International Frequency Control Symposium Joint with the 22nd European Frequency and Time Forum, 2009, pp. 50–53, https://doi.org/10.1109/FREQ.2009.5168140.
[40] S.M. Vaezi-Nejad, M. Cox, N. Cooper, Novel instrumentation for measurement of relative intensity noise, Trans. Inst. Meas. Control 34 (2012) 477–486, https://doi.org/10.1177/0142331211399330.
[41] E. Conforti, M. Rodigheri, T. Sutili, F.J. Galdieri, Acoustical and 1/f noises in narrow linewidth lasers, Opt Commun. 476 (2020) 126286, https://doi.org/10.1016/j.optcom.2020.126286.
[42] S. Huang, T. Zhu, M. Liu, W. Huang, Precise measurement of ultra-narrow laser linewidths using the strong coherent envelope, Sci. Rep. 7 (2017) 41988, https://doi.org/10.1038/srep41988.
[43] J. Li, H. Lee, K.J. Vahala, Microwave synthesizer using an on-chip Brillouin oscillator, Nat. Commun. 4 (2013) 2097, https://doi.org/10.1038/ncomms3097.
[44] T. Okoshi, K. Kikuchi, A. Nakayama, Novel method for high resolution measurement of laser output spectrum, Electron. Lett. 16 (1980) 630–631, https://doi.org/10.1049/el:19800437.
[45] L. Richter, H. Mandelberg, M. Kruger, P. McGrath, Linewidth determination from self-heterodyne measurements with subcoherence delay times, IEEE J. Quantum Electron. 22 (1986) 2070–2074, https://doi.org/10.1109/JQE.1986.1072909.
[46] E. Ip, A.P.T. Lau, D.J.F. Barros, J.M. Kahn, Coherent detection in optical fiber systems, Opt Express 16 (2008) 753–791, https://doi.org/10.1364/oe.16.000753.
[47] T.N. Huynh, L. Nguyen, L.P. Barry, Phase noise characterization of SGDBR lasers using phase modulation detection method with delayed self-heterodyne measurements, J. Lightwave Technol. 31 (2013) 1300–1308, https://doi.org/10.1109/JLT.2013.2247564.
[48] W.H. Burkett, B. Lu, M. Xiao, Influence of injection-current noise on the spectral characteristics of semiconductor lasers, IEEE J. Quantum Electron. 33 (1997) 2111–2118, https://doi.org/10.1109/3.641327.
[49] C. Henry, Performance of distributed feedback lasers designed to favor the energy gap mode, IEEE J. Quantum Electron. 21 (1985) 1913–1918, https://doi.org/10.1109/JQE.1985.1072611.
[50] J. Salzman, H. Olesen, A. Moller-Larsen, O. Albrektsen, J. Hanberg, J. Norregaard, B. Jonsson, B. Tromborg, Distributed feedback lasers with an S-bent waveguide for high-power single-mode operation, IEEE J. Sel. Top. Quantum Electron. 1 (1995) 346–355, https://doi.org/10.1109/2944.401214.
[51] L. Ge, O. Malik, H.E. Türeci, Enhancement of laser power-efficiency by control of spatial hole burning interactions, Nat. Photonics 8 (2014) 871–875, https://doi.org/10.1038/nphoton.2014.244.
[52] N. Opačak, B. Schwarz, Theory of frequency-modulated combs in lasers with spatial hole burning, dispersion, and Kerr nonlinearity, Phys. Rev. Lett. 123 (2019) 243902, https://doi.org/10.1103/PhysRevLett.123.243902.
[53] H. Bissessur, Effects of hole burning, carrier-induced losses and the carrier-dependent differential gain on the static characteristics of DFB lasers, J. Lightwave Technol. 10 (1992) 1617–1630, https://doi.org/10.1109/50.184901.
[54] J.E.A. Whiteaway, G.H.B. Thompson, A.J. Collar, C.J. Armistead, The design assessment of lambda/4 phase-shifted DFB laser structures, IEEE J. Quantum Electron. 25 (1989) 1261–1279, https://doi.org/10.1109/3.29257.
[55] C. Liu, B.L. Guan, G.X. Mi, L.Z.Y. Liao Yi-Ru, X.C. Li Jian-Jun, Li Jian-Jun, Xu Chen, A low threshold single transverse mode 852 nm semiconductor laser diode, Acta Phys. Sin. 66 (2017) 084205, https://doi.org/10.7498/aps.66.084205.
[56] A.A. Ballman, A.M. Glass, R.E. Nahory, H. Brown, Double doped low etch pit density InP with reduced optical absorption, J. Cryst. Growth 62 (1983) 198–202, https://doi.org/10.1016/0022-0248(83)90025-8.
[57] P. Prabhathan, V.M. Murukeshan, Z. Jing, P.V. Ramana, Compact SOI nanowire refractive index sensor using phase shifted Bragg grating, Opt Express 17 (2009) 15330–15341, https://doi.org/10.1364/oe.17.015330.

[58] M. Okai, M. Suzuki, T. Taniwatari, Strained multiquantum-well corrugation-pitch-modulated distributed feedback laser with ultranarrow (3.6 kHz) spectral linewidth, Electron. Lett. 29 (1993) 1696–1697, https://doi.org/10.1049/el:19931128.

[59] M. Okai, T. Tsuchiya, K. Uomi, N. Chinone, T. Harada, Corrugation-pitch modulated MQW-DFB lasers with narrow spectral linewidth, IEEE J. Quantum Electron. 27 (1991) 1767–1772, https://doi.org/10.1109/3.90002.

[60] K.-Y. Liou, N.K. Dutta, C.A. Burrus, Linewidth-narrowed distributed feedback injection lasers with long cavity length and detuned Bragg wavelength, Appl. Phys. Lett. 50 (1987) 489–491, https://doi.org/10.1063/1.98182.

[61] A.C. Tropper, S. Hoogland, Extended cavity surface-emitting semiconductor lasers, Prog. Quantum Electron. 30 (2006) 1–43, https://doi.org/10.1016/j.pquantelec.2005.10.002.

[62] P.B. Deotare, M.W. McCutcheon, I.W. Frank, M. Khan, M. Lončar, High quality factor photonic crystal nanobeam cavities, Appl. Phys. Lett. 94 (2009), https://doi.org/10.1063/1.3107263.

[63] M.T. Hill, M.C. Gather, Advances in small lasers, Nat. Photonics 8 (2014) 908–918, https://doi.org/10.1038/nphoton.2014.239.

[64] Y. Takahashi, Y. Inui, M. Chihara, T. Asano, R. Terawaki, S. Noda, A micrometre-scale Raman silicon laser with a microwatt threshold, Nature 498 (2013) 470–474, https://doi.org/10.1038/nature12237.

[65] M. Peccianti, A. PasQuazi, Y. Park, B.E. Little, S.T. Chu, D.J. Moss, R. Morandotti, Demonstration of a stable ultrafast laser based on a nonlinear microcavity, Nat. Commun. 3 (2012) 765, https://doi.org/10.1038/ncomms1762.

[66] S.J.M. Kuppens, M.P. Van Exter, J.P. Woerdman, Quantum-limited linewidth of a bad-cavity laser, Phys. Rev. Lett. 72 (1994) 3815–3818, https://doi.org/10.1103/PhysRevLett.72.3815.

[67] J. Piprek, P. Abraham, J.E. Bowers, Cavity length effects on internal loss and quantum efficiency of multiquantum-well lasers, IEEE J. Sel. Top. Quantum Electron. 5 (1999) 643–647, https://doi.org/10.1109/2944.788430.

[68] S. Ogita, M. Hirano, H. Soda, M. Yano, H. Ishikawa, H. Imai, Dependence of spectral linewidth of DFB lasers on facet reflectivity, Electron. Lett. 23 (1987) 347–349, https://doi.org/10.1049/el:19870256.

[69] D. Lu, Q. Yang, H. Wang, Y. He, H. Qi, H. Wang, L. Zhao, W. Wang, Review of semiconductor distributed feedback lasers in the optical communication band, Chin. J. Lasers 47 (2020) 0701001, https://doi.org/10.3788/CJL202047.0701001.

[70] L. Li, L. Lu, S. Li, R. Guo, Y. Shi, X. Chen, Phase-shifted distributed feedback laser with linearly chirped grating fabricated by reconstruction equivalent chirp technique, Opt. Laser Technol. 61 (2014) 57–61, https://doi.org/10.1016/j.optlastec.2014.02.008.

[71] Y. Shi, S. Li, Y. Zhou, L. Lu, L. Li, Y. Feng, X. Chen, Improved λ/4 phase-shifted DFB semiconductor laser with spatial hole burning compensation using grating chirp, Opt. Laser Technol. 44 (2012) 2443–2448, https://doi.org/10.1016/j.optlastec.2012.04.001.

[72] X. Lang, P. Jia, Y. Chen, L. Qin, L. Liang, C. Chen, Y. Wang, X. Shan, Y. Ning, L. Wang, Advances in narrow linewidth diode lasers, Sci. China Inf. Sci. 62 (2019) 1–13, https://doi.org/10.1007/s11432-019-9870-0.

[73] J. Telkkala, J. Viheriala, M. BisterKarinen J, P. Melanen, M. Dumitrescu, M. Guina, Narrow linewidth 1.55 μm laterally-coupled DFB lasers fabricated using nanoimprint lithography, in: IPRM 2011 – 23rd International Conference on Indium Phosphide and Related Materials, Germany, Berlin, 2011, pp. 1–4.

[74] L. Hou, M. Haji, J. Akbar, J.H. Marsh, Narrow linewidth laterally coupled 1.55 μm AlGaInAs/InP distributed feedback lasers integrated with a curved tapered semiconductor optical amplifier, Opt. Lett. 37 (2012) 4525–4527, https://doi.org/10.1364/OL.37.004525.

[75] K. Dridi, A. Benhsaien, J. Zhang, T.J. Hall, Narrow linewidth 1550 nm corrugated ridge waveguide DFB lasers, IEEE Photonics Technol. Lett. 26 (2014) 1192–1195, https://doi.org/10.1109/LPT.2014.2318593.

[76] X. Dong, Z. Xie, Y. Song, K. Yin, Z. Luo, J. Duan, C. Wang, Highly sensitive torsion sensor based on long period fiber grating fabricated by femtosecond laser pulses, Opt. Laser Technol. 97 (2017) 248–253, https://doi.org/10.1016/j.optlastec.2017.07.004.

[77] K.-Y. Liou, N.K. Dutta, C.A. Burrus, Linewidth-narrowed distributed feedback injection lasers with long cavity length and detuned Bragg wavelength, Appl. Phys. Lett. 50 (1987) 489–491, https://doi.org/10.1063/1.98182.

[78] K. Kikuchi, Precise estimation of linewidth reduction in wavelength-detuned DFB semiconductor lasers, Electron. Lett. 24 (1988) 80–81, https://doi.org/10.1049/el:19880052.

[79] M. Aoki, K. Uomi, T. Tsuchiya, S. Sasaki, M. Okai, N. Chinone, Quantum size effect on longitudinal spatial hole burning in MQW lambda/4-shifted DFB lasers, IEEE J. Quantum Electron. 27 (1991) 1782–1789, https://doi.org/10.1109/3.90004.

[80] E. Alkhazraji, W.W. Chow, F. Grillot, J.E. Bowers, Y. Wan, Linewidth narrowing in self-injection-locked on-chip lasers, Light Sci. Appl. 12 (2023) 162, https://doi.org/10.1038/s41377-023-01172-9.

[81] T. Yamanaka, K. Wakita, K. Yokoyama, Pure strain effect on reducing the chirp parameter in InGaAsP/InP quantum well electroabsorption modulators, Appl. Phys. Lett. 70 (1997) 87–89, https://doi.org/10.1063/1.119316.

[82] C.S. Chang, S.L. Chuang, Modeling of strained quantum-well lasers with spin-orbit coupling, IEEE J. Sel. Top. Quantum Electron. 1 (1995) 218–229, https://doi.org/10.1109/2944.401200.

[83] L.J. Mawst, H. Kim, G. Smith, W. Sun, N. Tansu, Strained-layer quantum well materials grown by MOCVD for diode laser application, Prog. Quantum Electron 75 (2021) 100303, https://doi.org/10.1016/j.pquantelec.2020.100303.

[84] S. Matsuo, T. Sato, K. Takeda, A. Shinya, K. Nozaki, E. Kuramochi, H. Taniyama, M. Notomi, T. Fujii, K. Hasebe, T. Kakitsuka, Photonic crystal lasers using wavelength-scale embedded active region, J. Phys. D Appl. Phys. 47 (2014) 023001, https://doi.org/10.1088/0022-3727/47/2/023001.

[85] Z. Lv, X. Zhao, Y. Sun, G. Tao, P. Du, S. Zhou, Unexpectedly simultaneous increase in wavelength and output power of yellow LEDs based on staggered quantum wells by Tmin flux modulation, Nanomater. (Basel). 12 (2022) 3378, https://doi.org/10.3390/nano12193378.

[86] Y. Iwata, R.G. Banal, S. Ichikawa, M. Funato, Y. Kawakami, Emission mechanisms in Al-rich AlGaN/AlN Quantum wells assessed by excitation power dependent photoluminescence spectroscopy, J. Appl. Phys. 117 (2015), https://doi.org/10.1063/1.4908282.

[87] T. Ohtoshi, N. Chinone, Linewidth enhancement factor in strained quantum well lasers, IEEE Photonics Technol. Lett. 1 (1989) 117–119, https://doi.org/10.1109/68.36007.

[88] M.C. Tatham, I.F. Lealman, C.P. Seltzer, L.D. Westbrook, D.M. Cooper, Resonance frequency, damping, and differential gain in 1.5 mu m multiple quantum-well lasers, IEEE J. Quantum Electron. 28 (1992) 408–414, https://doi.org/10.1109/3.123267.

[89] S. Suchalkin, D. Westerfeld, D. Donetski, S. Luryi, G. Belenky, R. Martinelli, I. Vurgaftman, J. Meyer, Optical gain and loss in 3-μm diode "W" quantum-well lasers, Appl. Phys. Lett. 80 (2002) 2833–2835, https://doi.org/10.1063/1.1471571.

[90] M. Rattunde, J. Schmitz, R. Kiefer, J. Wagner, Comprehensive analysis of the internal losses in 2.0μm (AlGaIn)(AsSb) quantum-well diode lasers, Appl. Phys. Lett. 84 (2004) 4750–4752, https://doi.org/10.1063/1.1760216.

[91] J. Piprek, P. Abraham, J.E. Bowers, Cavity length effects on internal loss and quantum efficiency of multiquantum-well lasers, IEEE J. Sel. Top. Quantum Electron. 5 (1999) 643–647, https://doi.org/10.1109/2944.788430.

[92] Y.Q. Wu, X.H. Che, L. Zhang, et al., Design of high-power low-noise 1550 nm distributed feedback laser chip, Semicond, Technol. 46 (2021) 7.

[93] T. Nakamura, T. Okuda, R. Kobayashi, Y. Muroya, K. Tsuruoka, Y. Ohsawa, T. Tsukuda, S. Ishikawa, 1.3-/spl mu/m AlGaInAs strain compensated MQW-buried-heterostructure lasers for uncooled 10-gb/s operation, IEEE J. Sel. Top. Quantum Electron. 11 (2005) 141–148, https://doi.org/10.1109/JSTQE.2004.841691.

[94] S. Matsuo, A. Shinya, T. Kakitsuka, K. Nozaki, T. Segawa, T. Sato, Y. Kawaguchi, M. Notomi, High-speed ultracompact buried heterostructure photonic-crystal laser with 13 fJ of energy consumed per bit transmitted, Nat. Photonics 4 (2010) 648–654, https://doi.org/10.1038/nphoton.2010.177.

[95] Z. Cheng, F. Mu, X. Ji, T. You, W. Xu, T. Suga, X. Ou, D.G. Cahill, S. Graham, Thermal visualization of buried interfaces enabled by ratio signal and steady-state heating of time-domain thermoreflectance, ACS Appl. Mater. Interfaces 13 (2021) 31843–31851, https://doi.org/10.1021/acsami.1c06212.

[96] S. Matsuo, T. Kakitsuka, Low-operating-energy directly modulated lasers for short-distance optical interconnects, Adv. Opt Photon 10 (2018) 567–643, https://doi.org/10.1364/AOP.10.000567.

[97] T. Fujii, K. Takeda, H. Nishi, N.P. Diamantopoulos, T. Sato, T. Kakitsuka, T. Tsuchizawa, S. Matsuo, Multiwavelength membrane laser array using selective area growth on directly bonded InP on SiO 2/Si, Optica 7 (2020) 838–846, https://doi.org/10.1364/OPTICA.391700.

[98] T. Aihara, T. Hiraki, T. Fujii, K. Takeda, T. Kakitsuka, T. Tsuchizawa, S. Matsuo, Mach-zehnder modulator using membrane InGaAsP phase shifters and SOAs inside interferometer arms on Si photonics platform, in: Optical Fiber Communication Conference, Optica Publishing Group, 2020, https://doi.org/10.1364/OFC.2020.M2B.5.

[99] K. Takaki, T. Kise, K. Maruyama, K. Hiraiwa, N. Yamanaka, M. Funabashi, A. Kasukawa, High-power CW-DFB LDs for optical communications, Furukawa Rev. 23 (2003).

[100] J. Huang, H. Lu, H. Su, et al., Ultrahigh power (180mW), linearly polarized DFB lasers with narrow spectral linewidth (100kHz) for 1550nm WDM+100 km long-haul transmission, in: International Conference on Engineering and Meta, Engineering, Orlando, Florida, 2010, pp. 31–35.

[101] Y.G. Zhao, A. Nikolov, R. Dutt, 1550 nm DFB semiconductor lasers with high power and low noise, Physics and Simulation of Optoelectronic Devices XIX, SPIE 7933 (2011) 525–531.

[102] H. Soda, Y. Kotaki, H. Sudo, H. Ishikawa, S. Yamakoshi, H. Imai, Stability in single longitudinal mode operation in GaInAsP/InP phase-adjusted DFB lasers, IEEE J. Quantum Electron. 23 (1987) 804–814, https://doi.org/10.1109/JQE.1987.1073454.

[103] C. Feng, J. Zhang, K. Tian, P. Wang, M. Huang, Design of 1310nm DFB Laser with high power and low noise, Semicond. Optoelectron. 35 (2014) 577–580, 632.

[104] J. Guo, H. Li, X. Xiong, D. Zhou, L. Zhao, S. Liang, Single-mode InGaAsP/InP BH lasers based on high-order slotted surface gratings, Opt Lett. 49 (2024) 286–289, https://doi.org/10.1364/OL.513993.

[105] B.S. Ryvkin, E.A. Avrutin, Spatial hole burning in high-power edge-emitting lasers: a simple analytical model and the effect on laser performance, J. Appl. Phys. 109 (2011), https://doi.org/10.1063/1.3549155, 043101–043101.

[106] S. Ogita, Y. Kotaki, M. Matsuda, Y. Kuwahara, H. Ishikawa, Long-cavity multiple-phase-shift distributed feedback laser diode for linewidth narrowing, J. Lightwave Technol. 8 (1990) 1596–1604, https://doi.org/10.1109/50.59202.

[107] M. Faugeron, M. Tran, F. Lelarge, M. Chtioui, Y. Robert, E. Vinet, A. Enard, J. Jacquet, F. Van Dijk, High-power, low RIN 1.55-μm directly modulated DFB lasers for analog signal transmission, IEEE Photonics Technol. Lett. 24 (2011) 116–118.

[108] M. Faugeron, M. Tran, O. Parillaud, M. Chtioui, Y. Robert, E. Vinet, A. Enard, J. Jacquet, F. Van Dijk, High-power tunable dilute mode DFB laser with low RIN and narrow linewidth, IEEE Photonics Technol. Lett. 25 (2012) 7–10, https://doi.org/10.1109/LPT.2012.2225419.

[109] H. Hao Wang, R.K. Ruikang Zhang, D. dan Lu, B. Baojun Wang, Y. Yongguang Huang, W. Wei Wang, L. Lingjuan Zhao, 1.55-μm high-power high-speed directly modulated semiconductor laser array, Acta Opt. Sin. 39 (2019) 0914001, https://doi.org/10.3788/AOS201939.0914001.

[110] Y. Liu, Y.G. Huang, R.K. Zhang, Y. Liu, High-power CW-DFB laser for co-packaged optics, Semicond. Optoelectron. 43 (2022) 6, https://doi.org/10.16818/j.issn1001-5868.2022032904.

[111] M. Xiang, Y. Zhang, G. Li, C. Liu, Q. Chen, Q. Lu, L. Huang, M. Lu, J. DoneGan, W. Guo, Wide-waveguide high-power low-RIN single-mode distributed feedback laser diodes for optical communication, Opt Express 30 (2022) 30187–30197, https://doi.org/10.1364/OE.464598.

[112] R. Lang, K. Kobayashi, External optical feedback effects on semiconductor injection laser properties, IEEE J. Quantum Electron. 16 (1980) 347–355, https://doi.org/10.1109/JQE.1980.1070479.

[113] P. Bouyer, T.L. Gustavson, K.G. Haritos, M.A. Kasevich, Microwave signal generation with optical injection locking, Opt. Lett. 21 (1996) 1502–1504, https://doi.org/10.1364/ol.21.001502.

[114] K. Szymaniec, S. Ghezali, L. Cognet, A. Clairon, Injection locking of diode lasers to frequency modulated source, Opt Commun. 144 (1997) 50–54, https://doi.org/10.1016/S0030-4018(97)00390-8.

[115] R. Adler, A study of locking phenomena in oscillators, Proc. IRE 34 (1946) 351–357, https://doi.org/10.1109/JRPROC.1946.229930.

[116] L.J. Paciorek, Injection locking of oscillators, Proc. IEEE 53 (1965) 1723–1727, https://doi.org/10.1109/PROC.1965.4345.

[117] K. Kurokawa, Injection locking of microwave solid-state oscillators, Proc. IEEE 61 (1973) 1386–1410, https://doi.org/10.1109/PROC.1973.9293.

[118] R. Lang, K. Kobayashi, External optical feedback effects on semiconductor injection laser properties, IEEE J. Quantum Electron. 16 (1980) 347–355, https://doi.org/10.1109/JQE.1980.1070479.

[119] W. Liang, V.S. Ilchenko, A.A. Savchenkov, A.B. Matsko, D. Seidel, L. Maleki, Whispering-gallery-mode-resonator-based ultranarrow linewidth external-cavity semiconductor laser, Opt. Lett. 35 (2010) 2822–2824, https://doi.org/10.1364/OL.35.002822.

[120] W. Liang, V.S. Ilchenko, D. Eliyahu, A.A. Savchenkov, A.B. Matsko, D. Seidel, L. Maleki, Ultralow noise miniature external cavity semiconductor laser, Nat. Commun. 6 (2015) 7371, https://doi.org/10.1038/ncomms8371.

[121] W. Liang, D. Eliyahu, A. Savchenkov, A. Matsko, A low-RIN spectrally pure whispering-gallery-mode resonator-based semiconductor laser, IEEE Photonics Technol. Lett. 30 (2018) 1933–1936, https://doi.org/10.1109/LPT.2018.2872963.

[122] W. Jin, Q.F. Yang, L. Chang, B. Shen, H. Wang, M.A. Leal, L. Wu, M. Gao, A. Feshali, M. Paniccia, K.J. Vahala, J.E. Bowers, Hertz-linewidth semiconductor lasers using CMOS-ready ultra-high-Q microresonators, Nat. Photonics 15 (2021) 346–353, https://doi.org/10.1038/s41566-021-00761-7.

[123] A. Takuma, T. Hiraki, T. Fujiial, Heterogeneously integrated widely tunable laser using lattice filter and ring resonator on Si photonics platform, Opt Express 30 (2022) 15820–15829, https://doi.org/10.1364/OE.448059.

[124] C. Chen, F. Wei, X. Han, Q. Su, H. Pi, G. Xin, H. Wu, A. Stroganov, Y. Sun, W. Ren, X. Chen, Q. Ye, H. Cai, W. Chen, Hybrid integrated Si3N4 external cavity laser with high power and narrow linewidth, Opt Express 31 (2023) 26078–26091, https://doi.org/10.1364/OE.487850.

[125] C. Xiang, W. Jin, O. Terra, 3D integration enables ultralow-noise isolator-free lasers in silicon photonics, Nature 620 (2023) 78–85, https://doi.org/10.5281/zenodo.7894620.

[126] P.W. Juodawlkis, W. Loh, F.J. O'Donnell, M.A. Brattain, J.J. Plant, High-power ultralow-noise semiconductor external cavity lasers based on low-confinement optical waveguide gain media. Novel In-Plane Semiconductor Lasers, SPIE Proceedings 7616 (2010) 174–182, https://doi.org/10.1117/12.846662.

[127] W. Loh, F.J. O'Donnell, J.J. Plant, M.A. Brattain, L.J. Missaggia, P.W. Juodawlkis, Packaged, high-power, narrow-linewidth slab-coupled optical waveguide external cavity laser (SCOWECL), IEEE Photonics Technol. Lett. 23 (2011) 974–976, https://doi.org/10.1109/LPT.2011.2146245.

[128] P.A. Morton, M.J. Morton, High-power, ultra-low noise hybrid lasers for microwave photonics and optical sensing, J. Lightwave Technol. 36 (2018) 5048–5057, https://doi.org/10.1109/JLT.2018.2817175.

[129] G. Sun, F. Wei, L. Zhang, D. Chen, X. Zhang, G. Chen, G. Xin, H. Pi, F. Yang, H. Cai, R. Qu, Low-noise external cavity semiconductor lasers based on polarization-maintaining fiber Bragg gratings, Chin. J. Lasers 45 (2018) 0601004, https://doi.org/10.3788/CJL201845.0601004.

[130] X. Luo, C. Chen, Y. Ning, J. Zhang, J. Chen, X. Zhang, L. Li, H. Wu, Y. Zhou, L. Qin, L. Wang, Single polarization, narrow linewidth hybrid laser based on selective polarization mode feedback, Opt. Laser Technol. Appl. 10 (2022) 154, https://doi.org/10.1016/j.optlastec.2022.108340.

[131] H. Li, Z. Wang, L. Wang, Y. Tan, F. Chen, Optically pumped milliwatt whispering-gallery microcavity laser, Light Sci. Appl. 12 (2023) 223, https://doi.org/10.1038/s41377-023-01264-6.

[132] G. Zhao, Ş.K. Özdemir, T. Wang, L. Xu, E. King, G.L. Long, L. Yang, Raman lasing and Fano lineshapes in a packaged fiber-coupled whispering-gallery-mode microresonator, Sci. Bull. 62 (2017) 875–878, https://doi.org/10.1016/j.scib.2017.05.011.

[133] H. Zhang, S. Zhou, Y. Jiang, J. Li, W. Feng, Z. Lin, Analysis on FM-to-AM conversion induced by spatial filter in a high-power laser system, Chin. Opt Lett. 10 (2012) 4–8.

[134] Y.M. Blanter, M. Büttiker, Shot noise in mesoscopic conductors, Phys. Rep. 336 (2000) 1–166, https://doi.org/10.1016/S0370-1573(99)00123-4.

[135] T. Gurski, R. Ku, M. Zimmerman, Frequency stability considerations for a coherent laser radar using a master oscillator/power amplifier, IEEE J. Quantum Electron. 15 (1979) 984–986, https://doi.org/10.1109/JQE.1979.1070200.

[136] Z.R. Lü, Z.K. Zhang, H. Wang, Y. Ding, X. Yang, L. Meng, H. Chai H, T. Yang, Research progress on 1.3 μm semiconductor quantum-dot lasers, Chin. J. Lasers 47 (2020) 0701016, https://doi.org/10.3788/CJL202047.0701016.

[137] A. Radu, Laser field effect on the subband structure in semiconductor quantum wires with conical potential profile, UPB Sci. Bull. A. 74 (2012) 121–130.

[138] B.O. Alaydin, D. Altun, O. Ozturk, E. Ozturk, High harmonic generations triggered by the intense laser field in GaAs/AlxGa1-xAs honeycomb quantum well wires, Mater. Today Phys. 38 (2023) 101232, https://doi.org/10.1016/j.mtphys.2023.101232.

[139] X. Lang, P. Jia, Y. Chen, L. Qin, L. Liang, C. Chen, Y. Wang, X. Shan, Y. Ning, L. Wang, Advances in narrow linewidth diode lasers, Sci. China Inf. Sci. 62 (2019) 1–3, https://doi.org/10.1007/s11432-019-9870-0.

[140] Q. Cui, Y. Lei, Y. Chen, C. Qiu, Y. Wang, D. Zhang, L. Fan, Y. Song, P. Jia, L. Liang, Y. Wang, L. Qin, Y. Ning, L. Wang, Advances in wide-tuning and narrow-linewidth external-cavity diode lasers, Sci. China Inf. Sci. 65 (2022) 181401, https://doi.org/10.1007/s11432-021-3454-7.
[141] B. Kelleher, M. Dillane, E.A. Viktorov, Optical information processing using dual state quantum dot lasers: complexity through simplicity, Light Sci. Appl. 10 (2021) 238, https://doi.org/10.1038/s41377-021-00670-y.
[142] X.J. Wang, H.H. Fang, Z.Z. Li, D. Wang, H.B. Sun, Laser manufacturing of spatial resolution approaching quantum limit, Light Sci. Appl. 13 (2024) 6, https://doi.org/10.1038/s41377-023-01354-5.
[143] A. Mittelstädt, A. Schliwa, P. Klenovský, Modeling electronic and optical properties of III–V quantum dots—selected recent developments, Light Sci. Appl. 11 (2022) 17, https://doi.org/10.1038/s41377-021-00700-9.
[144] B. Dong, M. Dumont, O. Terra, H. Wang, A. Netherton, J.E. Bowers, Broadband quantum-dot frequency-modulated comb laser, Light Sci. Appl. 12 (2023) 182, https://doi.org/10.1038/s41377-023-01225-z.
[145] M. Mohammadimasoudi, P. Geiregat, F. Van Acker, J. Beeckman, Z. Hens, T. Aubert, K. Neyts, Quantum dot lasing from a waterproof and stretchable polymer film, Light Sci. Appl. 11 (2022) 275, https://doi.org/10.1038/s41377-022-00960-z.